IEEE Access
Multidisciplinary | Rapid Review | Open Access Journal

Received 12 July 2022, accepted 7 August 2022, date of publication 18 August 2022, date of current version 26 August 2022.

Digital Object Identifier 10.1109/ACCESS.2022.3199737

RESEARCH ARTICLE

Research on Lossless Compression Coding Algorithm of N-Band Parametric Spectral Integer Reversible Transformation Combined With the Lifting Scheme for Hyperspectral Images

CHANGCHENG LI[1,2,3], DEYUN CHEN[1], CHENGJUN XIE[4], YILONG GAO[5], AND JINRUI LIU[2,3]

[1]School of Computer Science and Technology, Harbin University of Science and Technology, Harbin 150080, China
[2]School of Electrical and Information Engineering, Jilin Agricultural Science and Technology University, Jilin City 132101, China
[3]Smart Agricultural Engineering Research Center of Jilin Province, Jilin City 132101, China
[4]School of Computer Science and Technology, Beihua University, Jilin City 132103, China
[5]School of Information Science and Engineering, Linyi University, Linyi 276000, China

Corresponding authors: Changcheng Li (lichangcheng@jlnku.edu.cn) and Deyun Chen (934853276@qq.com)

This work was supported in part by the Natural Science Foundation of China under Project 60972127, Project 61072111, and Project 60672156; in part by the Key Scientific Research Project of Jilin Provincial Department of Education under Project JJKH20220390KJ; in part by the Key Project of Jilin Provincial Science and Technology Department under Project 20100503; and in part by the Project for Science and Technology Center and Science and Technology Service Platform under Project 20180623004TC.

ABSTRACT After considering the spectral correlation of structure and statistics of the hyperspectral image, the redundancy reduction is optimized using reversible transformation of integer matrices in conjunction with the N-band integer reversible transformation of spectral matrices. This paper proposes a new quantization algorithm, XCJRCT, that uses invertible matrix transformation to remove spectral redundancy and optimize bit allocation in structure. The lifting scheme of the discrete wavelet transform (DWT) is used in conjunction with other algorithms to reduce redundancy and set partitioning in hierarchical trees (SPIHT) coding. The experimental results show that lossless compression is significantly better than JPEG-LS, WinZip, ARJ, and DPCM. Using the Jet Propulsion Laboratory (JPL) Canal test image (Band Sequential) as an example data set, the average compression ratio increases by about 73.691598%, 67.713276%, 65.175242%, and 59.107580%, respectively, compared to the above algorithms.

INDEX TERMS Hyperspectral image, lossless compression, SPIHT algorithm, wavelet transform, XCJRCT transform.

I. INTRODUCTION

Hyperspectral images typically contain a large amount of data, for which compression becomes critical to reduce the required space, cost, transmission time, and processing time and thus improve their transmission and storage efficiency and lower their application costs. The spectral transformation is an important step in the image processing of multispectral and hyperspectral images because it can provide a high compression ratio, and hyperspectral image codes compression primarily focuses on redundancy reduction and codes algorithm.

To address the problem of congestion in aircraft and satellite downlinks, Báscones *et al.* [1] used vector quantization and principal component analysis (PCA) for spectral decorrelation of images. However, these methods only improved image storage and transmission for hyperspectral image compression. The limited accuracy improvement was obtained from high-compression, low signal-to-noise ratio (SNR) images to low-compression near-lossless images. Guerra *et al.* [2] proposed a lossy compression algorithm based on transforms for hyperspectral image systems (hyper LCA). Czajkowski *et al.* [3] proposed a new sampling

The associate editor coordinating the review of this manuscript and approving it for publication was Wenming Cao.

scheme based on a random selection of Morlet wavelets convolved with white noise, resulting in a shorter signal acquisition time. However, only at low resolutions was the compression ratio for single-pixel imaging slightly improved. Valsesia and Magli [4] investigated the performance of a lossless predictive compressor and a fast compression method based on image prequantization. Although a novel lossless compression method was proposed, its prediction was performed only in conjunction with the convolutional neural network, with no verification of lossless compression of reversible transformation. Blanes *et al.* [5] investigated the impact of parameter selection on the compression performance of the Consultative Committee for Space Data Systems (CCSDS) -123.0-B-2 Low-Complexity Multispectral and Hyperspectral Image Compression Standard (Lossless and Near-Lossless). However, because only related parameters were provided, the study was unable to further optimize the lossless compression method in terms of coding performance. Pflugfelder and Scharr [6] proposed a lossless affine transformation method for two-dimensional images, but its runtime was significantly longer than that of the toolbox algorithm, compromising the image quality obtained by hardware. Hernández-Cabronero *et al.* [7] were the first to combine the most competitive spectral decorrelation approach and the best-performing low-complexity compressor approach while considering only lossless compression, and they obtained the compression performance and execution time for a group of data in an actual remote sensing task. To improve the efficiency of an orbiting cloud screen targeting the spaceborne environment, Li *et al.* [8] proposed a new spectral-spatial classification strategy. The threshold exponential spectral angle map (TESAM), adaptive Markov random field (aMRF), and dynamic stochastic resonance were used to create hyperspectral images (DSR). Using only spectral information, classification performance was improved, allowing automatic spectrum settings of cloud covers for the ongoing Earth Observing-1 (EO-1) and related satellites. Liu and Chen [9] proposed an adaptive spectral decorrelation method based on clustering analysis, but they did not address the image compression issue of the moderate resolution imaging spectroradiometer (MODIS) Wang *et al.* [10] reconstructed images based on significant correlations in spatial and spectral dimensions that were intrinsic properties of the hyperspectral image, taking into account the notable advantages of coded aperture snapshot spectral imaging. However, no significant improvement in the lossless compression ratio of the compressive coding algorithm was observed. Xue *et al.* [11] proposed using structured sparsity before first characterizing spatial and spectral images before proposing no new scheme in terms of the compressive coding algorithm for hyperspectral images. [12] built a low computational complexity fast lossless compression model (WCCSDS123), which was suitable for hardware implementation. The method was only useful for the wedge filter spectral imager because it predicted the values of sampling points using the local sum and improved local difference vectors. Kong *et al.* [13] proposed an end-to-end multispectral image compression method based on a convolutional neural network and investigated multispectral image reconstruction in the inverse transformation process at the coding and decoding ends. Li *et al.* [14] used the Compute Unified Device Architecture (CUDA), a parallel computing platform and programming model developed by NVIDIA, to reduce the lossless compression time from 30-60 minutes to a few seconds with almost no loss in accuracy. Fu *et al.* [15] proposed a grouped multiscale dilated network structure to increase the receptive fields of each network layer, which was directly used for multi-band spectral image sharpening of other types. Zhu *et al.* [16] investigated the design and optimization of a perovskite quantum dot spectrometer using a total-variation compressive sensing approach. However, the approach only reconstructed the target spectrum in a quantum dot spectrometer coupling measurement by combining quantum dots with a single image sensor, revealing inherent photoluminescence emission defects and poor batch-to-batch repeatability. Liu and Wu [17] developed a lossless compression method for multispectral images in dynamic video capture limited to dynamic video acquisition scenarios. Zhu *et al.* [18] also proposed a lossless compression method for hyperspectral images based on adaptive band selection and an optimal prediction sequence, with an arithmetic encoder used to encode the prediction residual entropy. Li *et al.* [19] optimized the predictor of the CCSDS 123.0-B-1 algorithm, only using the optimized residual mapper to improve prediction accuracy and reduce the length of the compression code to address issues such as insufficient use of pixel position information and spectral correlation and a low compression ratio. Li and Gong [20] proposed a lossless compression method for spectral information in a remote sensing image database; this method was based on the extraction of vector quantization features, which was optimized using the Linde, Buzo, and Gray (LBG) algorithm. Hernandez-Cabronero *et al.* [21] used closed-loop quantization of prediction errors to achieve near-lossless compression and determined the predicted sample values using sample representatives, which may not be equal to the reconstructed sample values. As a result, the compressed data volume became much smaller than that achieved by CCSDS 123.0-B-1, and the quality of the decompressed images could be controlled at the same time.

The number of studies on hyperspectral image compression and coding technology in China and elsewhere is steadily increasing. From the standpoint of the compression principle, the essence of image compression is removing redundant image information in spectral spatial and temporal dimensions and encoding the data, resulting in faster transmission while reducing storage space. Because of the strong data correlation in both spatial and spectral dimensions between the hyperspectral infrared atmospheric image and the hyperspectral remote sensing image, most studies on the compression of hyperspectral infrared data are based on the compression approach for hyperspectral images.

As a result, in addition to exploring the correlation in the entire spectral range, we should also focus on mining the inherent correlation characteristics in each spectral region in the spectral domain and thus design a reasonable scheme to remove spectral redundancy. Furthermore, while the compression of hyperspectral images in the spectral-spatial dimension has received a lot of attention in the literature, only a few studies have focused on compression in the time dimension, with the majority of them referencing video compression algorithms. The data characteristics of hyperspectral images in the time dimension differ significantly from those of general video data, and traditional video compression algorithms are not entirely appropriate for hyperspectral infrared images. As a result, the distinct data properties of hyperspectral images in the time dimension should be thoroughly investigated. The CCSDS focuses on predictive coding-based lossless and near-lossless compression methods, and Lossless compression of hyperspectral images with reversible transformation must be evaluated. Furthermore, because of the detectors' improved time resolution, the daily acquired images have extremely high data redundancy. As a result, simply compressing hyperspectral images in spatial and spectral dimensions is far insufficient, and real-time compression methods should be studied online based on the existing relationships between images at different times, allowing for rapid image data transmission.

Based on the aforementioned analysis, this paper used three band parametric spectral integer reversible transformation in conjunction with wavelet lifting scheme transformation to remove spectral and spatial redundancy by implementing lossless compression of the hyperspectral image using SPIHT codes algorithm.

II. REDUNDANCY ELIMINATION TRANSFORMATION

A. XCJRCT TRANSFORM

Given that $|\det| = a \neq 1$, any invertible $n \times n$ matrix A, irrespective of the corresponding actual physical meaning of the transformation results, can be transformed into the matrix with 1 for the module of the determinant value by improving the transformational matrix. If the module of the determinant value of the matrix equals 1, matrix A has the basic definite triangular matrix decomposition. Therefore, it is possible to construct the N-band parametric spectral integer reversible transformation matrix, and the optimal transformation can be chosen according to the actual needs of the problem since there are infinite such integer reversible transformations. For example, the N-band parametric spectral reversible transformation is realized by the principle of the lowest energy. Matrix Theory states that the triangular decomposition is a necessary part of a nonsingular matrix with P, L, D, and U as the short forms for permutation matrix (P), unit lower triangular matrix (L), diagonal (D) matrix, and unit upper triangular (U) matrix $|\det D| = |\det \mathrm{PD}| = |\det \mathrm{PLDU}| = |\det A| = 1$, respectively which implies that the invertible transform matrix A can be found for $N \times N$ integer implementation. The results provided constructive proof, but without being parameterized, and any problem for optimum transform solution. We can conclude that the matrix reversible transformation of SHIRCT, RCT, YFbFr, YCbCr is not optimal for the well-known implementation of three-band spectral integers (R, G, B) spectral integer implementation [22]. This transformation is one of the main entry points to studying this problem. In this paper, the reversible matrix transformation realized by the three-band spectral integer was used as an example to illustrate the problem solving of optimal transformation to show the importance of the problem under study [23].

Set

$$T = \begin{bmatrix} 1 & & \\ & 1 & \\ a_1 & a_2 & 1 \end{bmatrix} \begin{bmatrix} 1 & & \\ b_1 & 1 & b_2 \\ & & 1 \end{bmatrix} \begin{bmatrix} 1 & c_1 & \\ & 1 & c_2 \\ & & 1 \end{bmatrix} \begin{bmatrix} 1 & & \\ & 1 & \\ d_1 & d_2 & 1 \end{bmatrix} \quad (1)$$

$$T = \begin{bmatrix} 1+c_2d_1 & c_1+c_2d_2 & c_2 \\ b_1(1+c_2d_1)+b_2d_1 & b_1(c_1+c_2d_2)+1+b_2d_2 & b_1c_2+b_2 \\ \Delta_1 & \Delta_2 & \Delta_3 \end{bmatrix} \quad (2)$$

Among $\Delta_1 = a_1 \times (1 + c_2 \times d_1) + \mathrm{a}_2 \times [b_1 \times (1 + c_2 \times d_1) + b_2 \times d_1] + d_1$, $\Delta_2 = a_1 \times (c_1 + c_2 \times d_2) + \mathrm{a}_2 \times [b_1 \times (c_1 + c_2 \times d_2) + 1 + b_2 \times d_2] + d_2$, $\Delta_3 = a_1 \times c_2 + \mathrm{a}_2 \times (b_1 \times c_2 + b_2) + 1$, Set $\mathrm{T} = \mathrm{P_L AP_R}$, Herewith

$$P_L = \begin{bmatrix} 1 & 0 & 0 \\ 1 & 0 & -1 \\ 0 & 1 & 0 \end{bmatrix} \quad (3)$$

$$P_R = \begin{bmatrix} 0 & 0 & 1 \\ 0 & 1 & 0 \\ 1 & 0 & 0 \end{bmatrix} \quad (4)$$

And,

$$A = \begin{bmatrix} c_2 & c_1+c_2d_2 & 1+c_2d_1 \\ -\Delta_1 & -\Delta_2 & -\Delta_3 \\ b_1c_2+b_2 & b_1(c_1+c_2d_2)+1+b_2d_d & b_1(1+c_2d_1)+b_2d_1 \end{bmatrix} \quad (5)$$

Formulas (1) and (2) show that the first two lines of the matrix are irrelevant to $a_1\mathrm{a}_1$ and a_2a_2, so the transformation of the invertible matrix of the integer implementation can be parameterized $b_1 = -0.5$, $b_2 = -0.1$, $c_1 = 1$, $c_2 = 0.5$, $d_1 = -0.5$, $d_2 = -0.5$, and

$$T = \begin{bmatrix} 0.75 & 0.75 & 0.5 \\ -0.34375 & 0.65625 & -0.3125 \\ \Delta_1 & \Delta_2 & \Delta_3 \end{bmatrix} \quad (6)$$

And,

$\Delta_1 = v0.75 \times a_1 - 0.34375 \times \mathrm{a}_2 - 0.5$, $\Delta_2 = 0.96875 \times a_1 + 0.65625 \times \mathrm{a}_2 - 0.5$, $\Delta_3 = 0.5 \times a_1 - 0.3125 \times \mathrm{a}_2 + 1 \Delta_3 = 0.5\mathrm{a}_1 - 0.3125\mathrm{a}_2 + 1$. To obtain the best effects, $\Delta_1 + \Delta_2 + \Delta_3 = 0$ $\Delta_1 + \Delta_2 + \Delta_3 = 0$ can be obtained from $a_1 =$

$0a_1 = 0$, and the parameterized transformation matrix can be deduced.

$$A = \begin{bmatrix} 0.5 & 0.75 & 0.75 \\ -0.3125a_2+1 & 0.65625a_2-0.5 & -0.34375a_2-0.5 \\ 0.3125 & -0.65625 & 0.34375 \end{bmatrix} \tag{7}$$

$a_2 = 0.75a_2 = 0.75$ and the well-known transformation of SHIRCT can be obtained [13].

If $Z = [Z_1, Z_2, Z_3]^T$, $X = [X_1, X_2, X_3]^T$, then $Z_2 = (0.3125 \times X_1 - 0.65625 \times X_2 + 0.34375 \times X_3) \times a_2 + X_1 - 0.5 \times (X_2 + X_3) = Z_3 \times a_2 + X_1 - 0.5 \times (X_2 + X_3)$, with the actual effect of image compression taken into account. Furthermore, because it is a parametric expression, $|Z_2|$ is expected to be the smallest possible; if Z_2 and $X_1 - 0.5 \times (X_2 + X_3)$ are all set values, then the different choice of a_2 to Z_2 has a significant influence; a_2 denotes the different reversible transformation. There are an infinite number of such reversible transformations in theory. However, the best transformation can always be chosen based on the needs of the current problem. For instance, consider the parametric 3-band spectral integer reversible transformation based on the principle of least energy. The current paper presented the following expression of the XCJRCT transform [24] for a three-band spectrum integer invertible transformation matrix:

Forward Transform,

$$\begin{aligned} d &= In_1 - ((In_2 + In_3) \gg 1) \\ Out_1 &= In_2 + In_3 + (d \gg 1) \\ Out_3 &= -I_2 + ((Out_1 + (d \gg 3)) \gg 1) \\ Out_2 &= d + (\gamma \times Out_3) \gg \lambda \end{aligned}$$

Inverse Transform,

$$\begin{aligned} d &= Out_2 - (\gamma \times Out_3) \gg \lambda \\ I_2 &= -Out_3 + ((Out_1 + (d \gg 3)) \gg 1) \\ I_3 &= Out_1 - n_2 + (d \gg 1) \\ In_1 &= d + ((In_2 + I_3) \gg 1) \end{aligned}$$

where d represents an intermediate variable, In_1, In_2, and In_3 represent three input signals, Out_1, Out_2, and Out_3 represent three output signals, and '$\gg$' represents a binary left shift symbol. The values of γ and λ are transformable parameters that can be evaluated based on the needs of the actual problem to be solved. For ease of hardware configuration, the above transforms can be performed with addition and shift.

Therefore, the quantization algorithm and DWT are combined to mine data redundancy. The parametric transformation in this paper is based on integer reversible transformation of three parameters. Presented the expression of a 3 band spectrum integer invertible transformation matrix as given below:

$$T = \begin{bmatrix} 1 & & \\ & 1 & \\ x_1 & x_2 & 1 \end{bmatrix} \times \begin{bmatrix} 1 & & \\ y_1 & 1 & y_2 \\ & & 1 \end{bmatrix} \times \begin{bmatrix} 1 & z_1 & z_2 \\ & 1 & \\ & & 1 \end{bmatrix} \times \begin{bmatrix} 1 & & \\ & 1 & \\ w_1 & w_2 & 1 \end{bmatrix} \tag{8}$$

Select the suitable algorithm to obtain;

$$T = \begin{bmatrix} 1 + z_2 \times w_1 & z_1 + z_2 \times w_2 & z_2 \\ y_1 \times (1 + z_2 \times w_1) + y_2 \times w_1 + y_2 \times w_2 + 1 & y_1 \times (z_1 + z_2 \times w_2) + y_1 \times z_2 + y_2 & \\ \delta_1 & \delta_2 & \delta_3 \end{bmatrix} \tag{9}$$

Among them, $\delta_1 = x_1 \times (1 + z_2 \times w_1) + x_2 \times [y_1 \times (z_1 + z_2 \times w_2) + y_2 \times w_2 + 1] + w_1$, $\delta_2 = x_1 \times (z_1 + z_2 \times w_2) + x_2 \times [y_1 \times (z_1 + z_2 \times w_2) + y_2 \times w_2 + 1] + w_2$, $\delta_3 = x_1 \times z_2 + x_2 \times (y_1 \times z_2 \times y_2) + 1$. Hence, γ and λ are adjustable parameters for transformations, x_1, x_2, y_1, y_2, z_1, z_2, $w1$, and w_2 are parameters for matrices of integer reversible transformation, and the different choice of parameters can lead to different matrices of integer reversible transformation.

B. LIFTING SCHEME OF WAVELET TRANSFORM

Discrete wavelet transformation (DWT) is now recognized as an excellent transformation for removing spatial redundancy, and understanding of DWT in removing spatial redundancy has matured; however, the use of DWT to remove spectral redundancy is not always the best, and in some cases is very poor [25]. For example, using DWT to remove spectral redundancy from a 7-band image with only one decomposition is far from the effects of redundancy reduction. This is because the number of bands involved in the DWT transformation is not a power of two, the boundary extension is unsuitable for DWT to eliminate spectral redundancy, and each extension adds one frame of image data. Such data are massive and will have a significant negative impact on redundancy. If removal of spectral redundancy is required, DWT can be used in conjunction with other transformations. DWT is used for a portion of the power of 2, while other transformations are used for the remainder. As a result, we propose a unified N-band parametric spectral integer-reversible transformation in this paper. The flexible N-band parametric spectral integer reversible transformation can be used alone to implement spectral redundancy reduction, or it can be combined with DWT or subtraction transformations. Furthermore, another significant benefit of the transformations mentioned above can be taken with addition and change to achieve the ease of hardware configuration with high computational speed.

The transformation of S, TS, $S + P$ may be seen as a special case of Sweden's lifting scheme. The wavelet transform process based on the lifting scheme may be divided into four types of transforms: decomposing, predicting, updating, and optimizing.

1) DECOMPOSING (LAZY WAVELET TRANSFORM OR POLYPHASE WAVELET TRANSFORM)

The original signal $S_{j,k}$ is divided into two disjoint subsets: $S_{j+1,k}$, and d_{j+1}. The original signal $S_{j,k}$ is usually conducted with a lazy wavelet and polyphase wavelet transform and decomposed into even and odd series, i.e.,

$$\text{split}(S_{j,k}) = (S_{j,2\,k}, S_{j,2k+1}) = (S_{j+1,k}, d_{j+1,k}).$$

2) PREDICTING (DUAL LIFTING STEP)

As $S_{j+1,k}$ can be predicted with $d_{j+1,k}$, according to the relativity between the data, a prediction operator, P, which is irrelevant to the structure of the data set, is used to obtain $d_{j+1,k} = P\left(S_{j+1,k}\right) \cdot d_{j+1,k}$ is used with different values between the prediction value $P\left(S_{j+1,k}\right)$ and itself to substitute $d_{j+1,k}$, and the differential value shows proximity between the above two values. If the prediction is reasonable, the differential value data set will consist of less information than the original subset $d_{j+1,k}$.

3) UPDATING (UPDATE LIFTING STEP)

Some properties (e.g., the mean value) of the coefficient subset $S_{j+1}k$ produced by the two previous steps are not consistent with those of the original data and therefore require an update process. The process is to use operator U to generate a better subset $S_{j+1,k}$ to maintain some features of the original data set $S_{j,k}$. In addition, $S_{j+1,k}$ is defined as $S_{j+1,k} = S_{j,2\,k+1} + U\left(d_{j+1,k}\right)$. After division through the processes of decomposing, predicting, and updating of $S_{j+1,k}$, $S_{j+1,k}$ can be divided into $d_{j+2,k}$, and $S_{j+2,k}$, The wavelet transform of the original data $S_{0,k}$ will be demonstrated as $\{S_J, d_J, d_J$ $1, \ldots\ldots, d_1\}$ after J times of decomposition, and S_J, among them, represents the low-frequency part of the signal, and $\{d_J, d_{J-1}, \ldots\ldots, d_1\}$ denotes the high-frequency part of the signal.

4) OPTIMIZING LIFTING STEP

Alternately, the dual lifting step and the update lifting step can be used to improve the properties of the wavelet transform in light of the current situation. The lifting-based forward transform algorithm can be expressed as follows:

$$S^0_{j+1,k} = S_{j,2k} \tag{10}$$

And,

$$d^0_{j+1,k} = S_{j,2k+1} \tag{11}$$

dual lifting step,

$$d^{(i)}_{j+1,k} = d^{i-1}_{j+1,k} - \sum_m p^{(i)}_m S^{(i-1)}_{j+1,k-m} \tag{12}$$

Update lifting step,

$$S^{(i)}_{j+1,k} = S^{(i-1)}_{j+1,k} - \sum_m u^{(i)}_m d^{(i)}_{j+1,k-m} \tag{13}$$

Even sample points, coupled with scale factors n_1 and n_h, become low-pass coefficients after M times operation of the update lifting step and dual lifting step, and odd sample points become high-pass coefficients, as shown in Formulas (14) and (15) below:

$$S_{j+1,k} = n_l S^{(M)}_{j+1,k} \tag{14}$$

$$d_{j+1,k} = n_h d^{(M)}_{j+1,k} \tag{15}$$

where M is the number of lifting steps; n_l and n_h are normalization factors, and for $n_l \times n_\mathrm{h} = 1$, respectively, and different

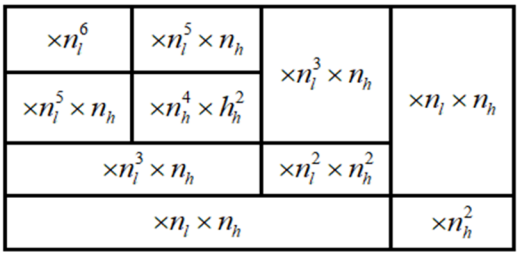

FIGURE 1. The implementation of normalization factors of the lifting scheme.

biorthogonal wavelets result in different values of n_1 and n_h. Figure 1 shows the normalization process after orthogonal transformation using the three-level wavelet transformation as an example.

The inverse transform may be written as:

$$S^{(M)}_{j+1,k} = \frac{S_{j+1,k}}{n_l} \tag{16}$$

$$d^{(M)}_{j+1,k} = \frac{d_{j+1,k}}{n_h} \tag{17}$$

$$S^{(i-1)}_{j+1,k} = S^{(i)}_{j+1,k} + \sum_m u^{(i)}_m d^{(i)}_{j+1,k-m} \tag{18}$$

$$d^{(i-1)}_{j+1,k} = d^{(i)}_{j+1,k} + \sum_m p^{(i)}_m S^{(i-1)}_{j+1,k-m} \tag{19}$$

Finally, the even-sample point and the odd-sample point are obtained, i.e., the even-sample point is as under:

$$S_{j,2k} = S^0_{j+1,k} \tag{20}$$

The odd point is given by,

$$S_{j,2k+1} = d^0_{j+1,k} \tag{21}$$

The lifting scheme is usually used to implement integer-integer wavelet transformation, i.e.

$$S_{j,2k} = \sum_m p^{(i)}_m S^{(i-1)}_{j+1,k-m} \tag{22}$$

$$S_{j,2k+1} = \sum_m u^{(i)}_m d^{(i)}_{j+1,k-m} \tag{23}$$

It can also be written as:

$$S_{j,2k} = \left\lfloor \sum_m p^{(i)}_m S^{(i-1)}_{j+1,k-m} \right\rfloor \tag{24}$$

$$S_{j,2k+1} = \left\lfloor \sum_m u^{(i)}_m d^{(i)}_{j+1,k-m} \right\rfloor \tag{25}$$

$\lfloor\rfloor$ To carry out the integer operation, the decomposition and reconstruction flow chart of the lifting scheme is indicated in Figure 2 shown below.

III. SPIHT ALGORITHM OF ENCODER AND DECODER

A. IMPLEMENTATION SCHEME FOR PARALLEL OPERATION OF ENCODER AND DECODER

The purpose of this research is to investigate the parallel coding structure in order to lay a solid foundation for the

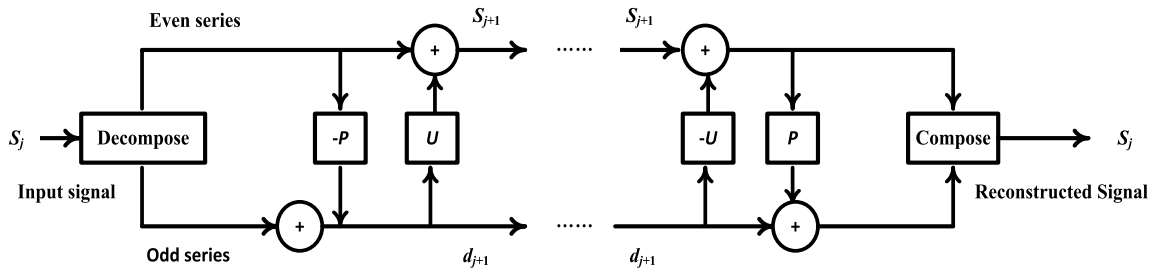

FIGURE 2. Decomposition and reconstruction of the lifting scheme.

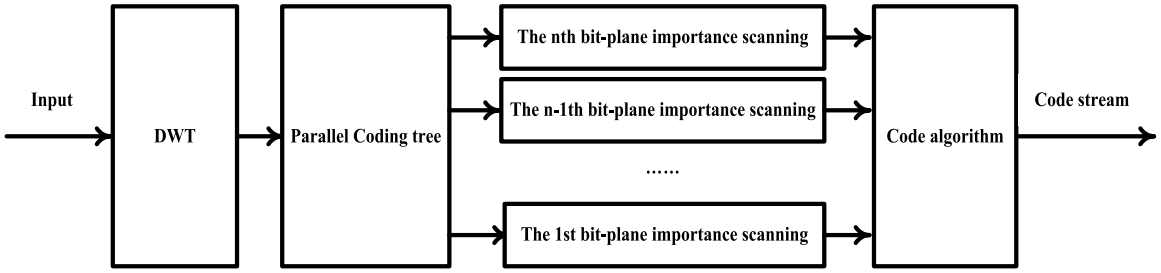

FIGURE 3. Parallel encoder based on DWT and bit-plane.

realization of encoder hardware. The study reveals that the magnitude of the bit planes after the DWT transformation is interrelated and fully predictable from the DWT coefficient. In other words, the logic or operation of the $i+1$ bit plane to the highest bit MSB at that pixel factor bit is the importance of the pixel coefficient relative to the current threshold of the i-bit plane. As a result, the bit plane can be thought of as sitting relatively independently, and the importance of each coefficient in each bit plane can be obtained simultaneously, allowing for parallel processing of the bit plane. Figure 3 shows the bit plane and the parallel encoder based on DWT.

The coding algorithm in Figure 3 employs SPIHT, which is modified according to the structure of the parallel coding tree.

B. ANTI-INTERFERENCE AND FAULT TOLERANCE SCHEME FOR ENCODER AND DECODER

The algorithm of the code of high robustness fault-tolerance is implemented in two aspects with the study of the anti-interference fault tolerance of code compression.

1) CODES ALGORITHM OF HYPERSPECTRAL IMAGE

The coding algorithm proposed in this article is used to divide the input data into independent packets of approximately the same length [26]. When a portion of these packages is lost, the receiving terminal uses the received packets to recover the information that is close to the lost portion. The number of packets received determines the quality of image recovery, not the nature or type of package received.

2) ROBUST WAVELET ZERO TREE IMAGE COMPRESSION WITH FIXED LENGTH PACKETIZATION

The output code stream of the wavelet zero tree encoder is divided into fixed-length fragments that can be decoded independently, and errors in one fragment do not affect other fragments, allowing different anti-interference and fault tolerance functions to be implemented [27]. The anti-interference and fault-tolerance scheme of the coding algorithm was proposed in this paper. Figure 4 shows the encoder and decoder's anti-interference and fault-tolerance scheme.

C. BASIC STEPS FOR SPIHT ALGORITHM

1) INITIALIZATION

Output

$$N = \lfloor \log_2(\max(i,j))\{|C_{i,j}|\} \rfloor \tag{26}$$

Set the LSP as an empty list, add the coordinates $(i, j) \epsilon H$ to the *LIP*, those with descendants (i.e., high-frequency sub-bands HL_J, LH_J, and HH_J) also to the *LIS*, as type *A* entries [28].

2) SORTING PROCESS

1. for each $(i, j) \epsilon$ *LIP, write*

Output $S_n(i, j)$;

If $S_n(i, j) = 1$ then add (i, j) to *LSP*, and output the signals of $C(i, j)$;

2. for each entry $(i, j) \epsilon$ *LIS, Do*

(1) If the entry is of type A, then

① Output $S_n(D(i, j))$;

② If $S_n(D(i, j)) = 1$, then for each $(k, l) \epsilon O(i, j)$, Do:

output $S_n(k, l)$;

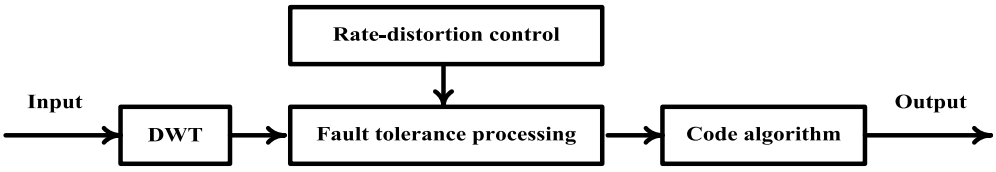

FIGURE 4. Anti-interference and fault-tolerance scheme for encoder and decoder.

If $S_n(k, l) = 1$, then add (k, l) to LSP, and output the signals of (k, l);

If $S_n(k, l) = 0$, then add (k, l) to the end of LIP;

③ If $L(i, j) \neq \phi$, then move (k, l) to the end of LIS as an entry of type B; otherwise, remove entry (i, j) from the LIS.

(2) If the entry is of type B, then

① Output $S_n(L(i, j))$;

② If $S_n(L(i, j)) = 1$, then

add each $(k, l) \epsilon O(i, j)$ to the end of the LIS as an entry of type A;

Remove (i, j) from the LIS.

3) REFINEMENT PROCESS

For each $(i, j) \epsilon LSP$ (except those just added above), the nth most significant bit of $|c_{i,j}|$ should be outputted.

4) UPDATE OF THE QUANTIZATION STEP

If $n = n - 1$; go to sorting process.

The management of the quantization steps is realized by the power dimensionality reduction of 2, and the quantization step size is updated by $n = n - 1$. Furthermore, the termination of the encoding algorithm is determined by the given bit rate. If it is noiseless compression, then the encoding will terminate until $n = 0$.

The output must be replaced with the input in such an algorithm for decoding [29].

IV. SIMULATION EXPERIMENT RESULTS AND DISCUSSION

A. OPTIMIZATION ANALYSIS OF TIME COMPLEXITY OF SPIHT ALGORITHM

To investigate the storage complexity and time complexity of the encoder and decoder algorithms, different encoder and decoder algorithms were tested under the same test conditions with the objective of optimizing memory storage [30]. In this paper, algorithm validation was conducted via simulations in Python 3.83. The Canal hyperspectral image test is provided with 24 test images of the 3-band color standard ($768 \times 512 \times 24$ bits) in the current study. The time complexity test of the SPIHT algorithm encoder and decoder is shown in Table 1.

Table 1: The test results show a huge difference in the time complexity of the SPIHT algorithm of encoder and decoder for hyperspectral Canal test images. Therefore, it is necessary to consider the cost-effectiveness ratio of the compression algorithm to choose the lossless compression coding algorithm.

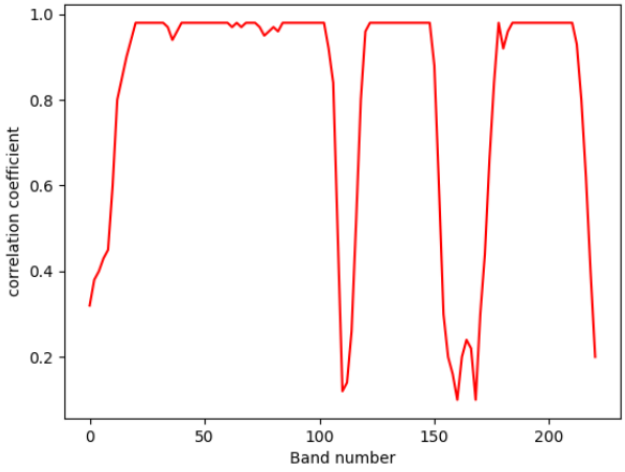

FIGURE 5. Correlation coefficients of adjacent frequency bands.

B. SIMULATION EXPERIMENT RESULTS

The test hyperspectral image, canal.bsq, has a spectral resolution of 10 nm, a spectral range of 400-2400 nm, 223 bands, and correlation coefficients R_i. Figure 5 shows the correlation coefficients of adjacent frequency bands.

The spectral correlation between the 106th-113th bands, the 152nd-157th bands, and the 217th-222nd bands has decreased significantly. The entire hyperspectral image is divided into five parts that can be transformed based on the different spectral correlation groups. The analysis demonstrates that previously published predictions and transformations to remove spectral redundancy were ineffective in improving the compression ratio. As a result, research is needed into the segmented matrix transformation to eliminate spectral redundancy and improve the effect of hyperspectral image compression.

As a result, the compression simulation experiment was performed with a 160-band canal.bsq (hyperspectral remote sensing image). The spectral and spatial joint transformation method is used to remove redundancy, employing the XCJRCT algorithm for spectral transformation, the wavelet transformation of the CDF (2, 2) lifting scheme for in-frame transformation, and SPIHT coding for transformation results.

Table 2 demonstrates the experimental results of the SPIHT compression coding experiment on the front 160- wavebands of the hyperspectral canal test image, canal.Bsq, conducted with SPIHT compression coding.

TABLE 1. Time complexity test of the SPIHT algorithm of encoder and decoder for hyperspectral Canal test images.

S. No	Test items	Time consumed for component 1 (second)	Time consumed for component 2 (second)	Time consumed for component 3 (second)	Total time consumed(second)
1	Encoding time	2.9986750	3.0959643	7.9754730	14.07011238
	Decoding time	2.2658303	2.3730757	6.3070387	10.94594474
2	Encoding time	3.2157974	2.8215273	6.7772356	12.81456034
	Decoding time	2.4562334	2.3001517	5.3591206	10.11550567
3	Encoding time	2.9566642	5.5280930	6.1404824	14.62523961
	Decoding time	2.2600787	4.4306617	4.7977326	11.48847293
4	Encoding time	3.1301487	6.1593783	6.8903447	16.17987172
	Decoding time	2.4928673	4.6744543	5.3084846	12.47580618
5	Encoding time	3.6245712	7.1992410	7.8736524	18.69746456
	Decoding time	2.9297278	5.6847013	6.1575124	14.77194147
6	Encoding time	3.7529566	5.5191863	7.5156246	16.78776749
	Decoding time	3.0190416	4.3855327	5.7820874	13.18666167
7	Encoding time	3.2416924	5.4628233	6.3943105	15.09882623
	Decoding time	2.6158501	4.0681253	4.9740756	11.65805096
8	Encoding time	4.1661656	7.7650073	8.0634594	19.99463233
	Decoding time	3.3876946	6.1349147	6.3631746	15.88578394
9	Encoding time	4.1565503	6.8231007	6.6824408	17.66209175
	Decoding time	3.3716007	5.1881470	5.2459116	13.80565928
10	Encoding time	6.5564910	6.9757907	6.7298522	20.26213386
	Decoding time	4.9604064	5.4944810	5.2783515	15.73323891
11	Encoding time	6.4981454	5.8957360	7.1784880	19.57236948
	Decoding time	4.9420302	4.4756970	5.6203453	15.03807248
12	Encoding time	5.0806405	5.1760320	6.6286462	16.8853187
	Decoding time	3.9141366	3.9981973	5.2364132	13.1487471
13	Encoding time	6.0295548	6.3974043	8.5770166	21.00397575
	Decoding time	4.5992092	4.8360363	6.8216742	16.25691971
14	Encoding time	5.7487864	6.1049823	7.5778661	19.43163484
	Decoding time	4.4206182	4.6787453	6.0106263	15.10998981
15	Encoding time	5.8115238	6.5384107	6.7576161	19.10755060
	Decoding time	4.4382564	4.9499113	5.1753948	14.56356260
16	Encoding time	5.6697458	5.5724533	6.7355815	17.97778064
	Decoding time	4.3167646	4.2450890	5.3085902	13.87044371
17	Encoding time	6.0520411	6.6584283	6.8170757	19.52754513
	Decoding time	4.5673372	5.2182217	5.3129963	15.09855516
18	Encoding time	7.0394882	7.3922343	8.3148695	22.74659203
	Decoding time	5.4674710	5.8011670	7.4982360	18.76687396
19	Encoding time	3.6871321	6.8659617	4.3921276	14.94522137
	Decoding time	2.9017248	5.3809167	3.5485314	11.83117287
20	Encoding time	3.4282746	6.3445533	3.9607810	13.73360902
	Decoding time	2.6830478	4.7024060	3.1615105	10.54696427
21	Encoding time	3.7689533	7.1299963	4.6561333	15.55508295
	Decoding time	2.9901484	5.5388003	3.6422327	12.17118145
22	Encoding time	3.810352154	6.7523290	7.8701886	18.43286978
	Decoding time	2.976459392	5.3042480	6.2390836	14.51979104
23	Encoding time	3.346880865	6.2293357	6.5725479	16.14876444
	Decoding time	2.627166302	4.8788917	5.1268319	12.63288982
24	Encoding time	3.631048825	6.4631650	7.9487521	18.04296588
	Decoding time	2.837301575	5.0115120	6.2421428	14.09095636

This paper highlights the experimental contrast between other lossless compressional algorithms and other classical lossless compression algorithms. The JPEG-lossless algorithm is based on the Lossless Compression for Images (LOCO-I) algorithm [31], which employs context modeling and error feedback to reduce the entropy of error images and perform run-length encoding on error images. At identical compression ratios for JPEG-LS, optimized transforms produce images that are more similar to the original than other state-of-the-art transforms [32].

On the 160 wavebands, which were divided into ten groups, SPIHT compression encoding was used, with 1D-CDF (2, 2) DWT for spectral compression and 2D-CDF (2, 2) DWT for in-frame compression. Figure 6 shows the change curve of the lossless compression ratio in relation to the previous 160 wavebands of the hyperspectral image canal.bsq.

WinZip is a famous method of lossless image compression [33]. ARJ utilizes a one-way self-adaptive Huffman lossless compression algorithm [34]. The difference pulse code

TABLE 2. The experimental results of the front 160- wavebands of the hyperspectral standard canal test image, canal.bsq, conducted with SPIHT compression coding.

Band number	Compression ratio	Band number	Compression ratio	Band number	Compression ratio	Band number	Compression ratio
1	1.755541	41	2.329984	81	2.224323	121	3.296251
2	1.633353	42	2.070715	82	3.038821	122	3.218150
3	1.591628	43	2.551834	83	2.736259	123	2.048760
4	1.923354	44	2.380882	84	1.980541	124	3.863241
5	1.813853	45	2.100785	85	3.023203	125	3.640335
6	1.574865	46	2.562296	86	3.006954	126	2.409639
7	2.067718	47	2.422921	87	2.411963	127	3.766124
8	1.939488	48	2.039672	88	3.123536	128	3.652968
9	1.718398	49	2.780095	89	2.931692	129	2.984963
10	2.188723	50	2.522625	90	2.368055	130	4.030227
11	2.055551	51	2.142991	91	2.895718	131	3.595506
12	1.817397	52	2.774117	92	2.855103	132	2.949526
13	2.328492	53	2.653400	93	1.753502	133	4.002802
14	2.161403	54	2.304878	94	2.551509	134	3.619254
15	1.905579	55	3.159807	95	2.836879	135	3.054718
16	2.410510	56	2.738319	96	2.356754	136	4.063182
17	2.261101	57	2.000350	97	2.986858	137	3.665017
18	1.995361	58	3.073849	98	2.701790	138	3.056118
19	2.537588	59	2.602811	99	2.330120	139	3.985652
20	2.343567	60	1.903991	100	3.030188	140	3.690207
21	2.067825	61	2.690342	101	2.945833	141	3.006389
22	2.572844	62	2.556727	102	2.525811	142	3.913511
23	2.422261	63	1.753655	103	2.754062	143	3.622532
24	2.138809	64	3.402952	104	2.991437	144	2.893833
25	2.625016	65	3.047503	105	2.052440	145	3.789494
26	2.417576	66	2.038424	106	3.064547	146	3.484321
27	2.170021	67	3.355705	107	2.735978	147	2.742638
28	2.507051	68	3.051106	108	1.960688	148	3.369272
29	2.423141	69	2.662673	109	3.963732	149	3.393713
30	2.165498	70	3.212722	110	3.569039	150	2.622091
31	2.334608	71	3.002665	111	2.616346	151	3.273188
32	2.040452	72	2.603997	112	3.953155	152	3.204101
33	1.672730	73	3.069721	113	3.667538	153	2.638000
34	2.360857	74	3.032141	114	3.056118	154	3.567765
35	2.326799	75	2.374803	115	3.718336	155	3.345601
36	1.890761	76	2.411891	116	3.671746	156	2.570281
37	2.399736	77	2.651729	117	2.810864	157	3.295436
38	2.312607	78	1.879081	118	3.930431	158	3.141690
39	1.799411	79	3.190810	119	3.464553	159	2.735230
40	2.360160	80	2.924618	120	2.723219	160	3.008650

modulation (DPCM) method is a traditional prediction-based lossless compression algorithm [14].

Table 3 shows the results of the comparison experiment between the algorithm proposed in this paper and the classical algorithm.

The experimental results reveal that the lossless compression ratio of each band increases faster with the change in the band, the compression ratio changes in the range of 1.574865–4.063182. The compression ratio of the proposed scheme is 2.728695, which is improved by about 73.691598%, 67.713276%, 65.175242%, and 59.107580%, in contrast to the classical algorithms, such as JPEG-LS, WinZip, ARJ, and DPCM, respectively. Therefore, the XCJRCT wavelet lifting scheme is very effective. It is of great significance for future applications of hyperspectral images. The hyperspectral images are multi-band images with a large amount of extremely valuable data, causing bandwidth constraints in information transmission. Therefore, the proposed XCJRCT wavelet lifting scheme has important research values for lossless hyperspectral image compression.

C. EXPERIMENT RESULTS AND DISCUSSION

This paper presents a comparative study of key spectral correlation techniques, both in China and elsewhere, in terms of the spectral characteristics of the lossless compression coding algorithm of the hyperspectral image. The simulation experiment shows the time complexity of the SPIHT algorithm of both encoder and decoder on canal hyperspectral test image using XCJRCT's 3-band spectral integer reversible transformation matrix in combination with the wavelet transformation lifting scheme and the SPIHT algorithm of encoder and decoder. The time complexity test of the SPIHT algorithm of encoder and decoder on the Canal hyperspectral test image is implemented using experimental results from the SPIHT algorithm of encoder and decoder on the first 160 bands of the hyperspectral standard test image canal.bsq. Furthermore, a comparison experiment with the classical lossless compression algorithm demonstrates that the scheme proposed in this paper is more efficient with a higher compression ratio than other methods.

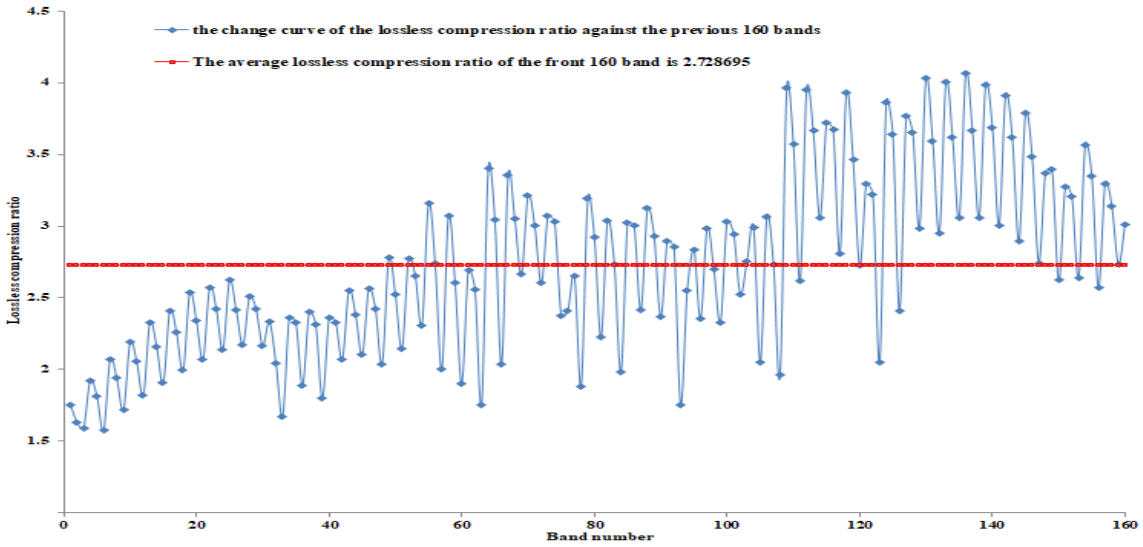

FIGURE 6. The change curve of the lossless compression ratio against the previous 160 bands of the hyperspectral image canal.bsq.

TABLE 3. The results of the contrast experiment with the algorithm proposed in this paper and the classical algorithm are presented.

Classical Algorithm	Compression ratio	Improvement of the proposed scheme against listed algorithms (dB)	Improvement of the Proposed Scheme against List Algorithms (%)
JPEG-LS	1.571	1.157695	73.691598%
WinZip	1.627	1.101695	67.713276%
ARJ	1.652	1.076695	65.175242%
DPCM	1.715	1.013695	59.107580%
The proposed scheme	2.728695		

As a result of the specificity and periodicity of the data collected by the target, the choice of parameters can be determined by applying the hyperspectral image in different fields, according to the materialization principle.

V. CONCLUSION

Hyperspectral remote sensing images have promising applications in agriculture, geography, resources, and the military. For example, in the field of agriculture engineering, the use of spectral detection sensors can provide timely and accurate information on the nutrient content of the soil; the use of correlation analysis can extract the combinations of the sensitive bands and the featured bands of the available phosphorus content; and the wavelet transformation of reflectance of hyperspectral image data. In addition, a spectral diagnostic model of available phosphorus in soil has been established based on various combinations of sensitive bands. Spectral technology and computer vision technology methods add more practical value to the study of the automatic detection method of ecological factors in crop environments, as well as the analysis of the characteristics of spectral and image data.

Overall, this paper proposes the XCJRCT transform in conjunction with the lifting wavelet transform scheme as the algorithm for the code for lossless compression of hyperspectral images. This effectively achieves lossless hyperspectral image compression, provides a high-efficiency algorithm for the development of spectral detection sensor hardware in the engineering field, and enables spectral detection sensors to capture, transmit, identify, and return information on environmental ecological factors in real time.

ACKNOWLEDGMENT

Author Contributions: Changcheng Li and Deyun Chen carried out the conceptualization studies, participated in the methodology alignment and drafted the manuscript. Chengjun Xie participated in the design of the study and performed the data curation. Yilong Gao and Jinrui Liu conceived of the study, and participated in its design and coordination and formal analysis. All authors read and approved the final manuscript. Data Availability: The authors declare that data supporting the findings of this study are available within the paper.

REFERENCES

[1] D. Báscones, C. González, and D. Mozos, "Hyperspectral image compression using vector quantization, PCA and JPEG2000," *Remote Sens.*, vol. 10, no. 6, p. 907, Jun. 2018.

[2] R. Guerra, Y. Barrios, M. Díaz, L. Santos, S. López, and R. Sarmiento, "A new algorithm for the on-board compression of hyperspectral images," *Remote Sens.*, vol. 10, no. 3, p. 428, Mar. 2018.

[3] K. M. Czajkowski, A. Pastuszczak, and R. Kotyński, "Single-pixel imaging with Morlet wavelet correlated random patterns," *Sci. Rep.*, vol. 8, no. 1, pp. 1–8, Dec. 2018.

[4] D. Valsesia and E. Magli, "High-throughput onboard hyperspectral image compression with ground-based CNN reconstruction," *IEEE Trans. Geosci. Remote Sens.*, vol. 57, no. 12, pp. 9544–9553, Dec. 2019.
[5] I. Blanes, A. Kiely, M. Hernández-Cabronero, and J. Serra-Sagristà, "Performance impact of parameter tuning on the CCSDS-123.0-B-2 low-complexity lossless and near-lossless multispectral and hyperspectral image compression standard," *Remote Sens.*, vol. 11, no. 11, p. 1390, Jun. 2019.
[6] D. Pflugfelder and H. Scharr, "Practically lossless affine image transformation," *IEEE Trans. Image Process.*, vol. 29, pp. 5367–5373, 2020.
[7] M. Hernández-Cabronero, J. Portell, I. Blanes, and J. Serra-Sagristà, "High-performance lossless compression of hyperspectral remote sensing scenes based on spectral decorrelation," *Remote Sens.*, vol. 12, no. 18, p. 2955, Sep. 2020.
[8] H. Li, H. Zheng, C. Han, H. Wang, and M. Miao, "Onboard spectral and spatial cloud detection for hyperspectral remote sensing images," *Remote Sens.*, vol. 10, no. 1, p. 152, Jan. 2018.
[9] F. Liu and Z. Chen, "An adaptive spectral decorrelation method for lossless MODIS image compression," *IEEE Trans. Geosci. Remote Sens.*, vol. 57, no. 2, pp. 803–814, Feb. 2019.
[10] L. Wang, T. Zhang, Y. Fu, and H. Huang, "HyperReconNet: Joint coded aperture optimization and image reconstruction for compressive hyperspectral imaging," *IEEE Trans. Image Process.*, vol. 28, no. 5, pp. 2257–2270, May 2019.
[11] J. Xue, Y. Zhao, W. Liao, and J. C.-W. Chan, "Hyper-Laplacian regularized nonlocal low-rank matrix recovery for hyperspectral image compressive sensing reconstruction," *Inf. Sci.*, vol. 501, pp. 406–420, Oct. 2019.
[12] H. Li, B. Hu, L. Yu, R. Wei, and T. Yu, "A fast lossless data compression method for the wedge filter spectral imager," *Spectrosc. Spectral Anal.*, vol. 39, no. 1, pp. 297–302, 2019.
[13] F. Kong, Y. Zhou, Q. Shen, and K. Wen, "End-to-end multispectral image compression using convolutional neural network," *Chin. J. Lasers*, vol. 46, no. 10, pp. 285–293, 2019.
[14] J. Li, J. Wu, and G. Jeon, "GPU acceleration of clustered DPCM for lossless compression of hyperspectral images," *IEEE Trans. Ind. Informat.*, vol. 16, no. 5, pp. 2906–2916, May 2020.
[15] X. Fu, W. Wang, Y. Huang, X. Ding, and J. Paisley, "Deep multiscale detail networks for multiband spectral image sharpening," *IEEE Trans. Neural Netw. Learn. Syst.*, vol. 32, no. 5, pp. 2090–2104, May 2021.
[16] X. Zhu, L. Bian, H. Fu, L. Wang, B. Zou, Q. Dai, J. Zhang, and H. Zhong, "Broadband perovskite quantum dot spectrometer beyond human visual resolution," *Light, Sci. Appl.*, vol. 9, no. 1, pp. 1–9, Dec. 2020.
[17] X. Liu and S. Wu, "Lossless compression of multispectral images in dynamic video capture," *Laser J.*, vol. 41, no. 8, pp. 87–90, 2020.
[18] F. Zhu, H. Wang, L. Yang, and C. Li, "Hyperspectral image lossless compression using adaptive bands selection and optimal prediction sequence," *Opt. Precis. Eng.*, vol. 28, no. 7, pp. 1609–1617, 2020.
[19] J. Li, W. Zhu, and F. Meng, "Hyperspectral image compression through reducing mapping prediction residuals," *Comput. Eng. Sci.*, vol. 42, no. 5, pp. 825–834, 2020.
[20] M. Li and J. Gong, "Study on method of spectral information in remote sensing image database," *J. Inner Mongolia Univ. Nat. Natural Sci.*, vol. 35, no. 3, pp. 215–220, 2020.
[21] M. Hernandez-Cabronero, A. B. Kiely, M. Klimesh, I. Blanes, J. Ligo, E. Magli, and J. Serra-Sagristà, "The CCSDS 123.0-B-2 'low-complexity lossless and near-lossless multispectral and hyperspectral image compression' standard: A comprehensive review," *IEEE Geosci. Remote Sens. Mag.*, vol. 9, no. 4, pp. 102–119, Dec. 2021.
[22] Y. Tan, J. Qin, X. Xiang, W. Ma, W. Pan, and N. N. Xiong, "A robust watermarking scheme in YCbCr color space based on channel coding," *IEEE Access*, vol. 7, pp. 25026–25036, 2019.
[23] C. Xie, "Lifting scheme," in *Wavelet Analysis: Theory and Applications*. Changchun, China: Northeast Normal Univ. Press, 2007, pp. 111–113.
[24] C. Li, C. Xie, Y. Tang, D. Chen, Y. Wang, and Z. Yu, "A lossless remote sensing hyperspectral image compression coding system," China Patent 11 303 814 3A, Jun. 25, 2021.
[25] V. A. Pimpalkhute, R. Page, A. Kothari, K. M. Bhurchandi, and V. M. Kamble, "Digital image noise estimation using DWT coefficients," *IEEE Trans. Image Process.*, vol. 30, pp. 1962–1972, 2021.
[26] Y. Fu, T. Zhang, L. Wang, and H. Huang, "Coded hyperspectral image reconstruction using deep external and internal learning," *IEEE Trans. Pattern Anal. Mach. Intell.*, vol. 44, no. 7, pp. 3404–3420, Jul. 2021.
[27] T. Brahimi, F. Khelifi, F. Laouir, and A. Kacha, "A new, enhanced EZW image codec with subband classification," *Multimedia Syst.*, vol. 28, no. 1, pp. 1–19, Feb. 2022.
[28] C. Xie and Y. Tian, "Research of lossless hyper-spectral image compression algorithm based on the combination of DWT transform and substraction transform," *Comput. Sci.*, vol. 35, no. 1, pp. 255–257, 2008.
[29] Y. A. Salih, A. A. Mohammed, and L. E. George, "Improved image compression scheme using hybrid encoding algorithm," *Kurdistan J. Appl. Res.*, vol. 4, no. 2, pp. 90–101, Oct. 2019.
[30] K. Dhou, "An innovative design of a hybrid chain coding algorithm for bi-level image compression using an agent-based modeling approach," *Appl. Soft Comput.*, vol. 79, pp. 94–110, Jun. 2019.
[31] C.-A. Chen, S.-L. Chen, C.-H. Lioa, and P. A. R. Abu, "Lossless CFA image compression chip design for wireless capsule endoscopy," *IEEE Access*, vol. 7, pp. 107047–107057, 2019.
[32] M. Hernández-Cabronero, V. Sanchez, I. Blanes, F. Aulí-Llinàs, M. W. Marcellin, and J. Serra-Sagristà, "Mosaic-based color-transform optimization for lossy and lossy-to-lossless compression of pathology whole-slide images," *IEEE Trans. Med. Imag.*, vol. 38, no. 1, pp. 21–32, Jan. 2019.
[33] M. M. Verstraete, L. A. Hunt, H. De Lemos, and L. Di Girolamo, "Replacing missing values in the standard multi-angle imaging spectroradiometer (MISR) radiometric camera-by-camera cloud mask (RCCM) data product," *Earth Syst. Sci. Data*, vol. 12, no. 1, pp. 611–628, Mar. 2020.
[34] L. Yan, J. Han, R. Xu, and Z. Li, "Model-free lossless data compression for real-time low-latency transmission in smart grids," *IEEE Trans. Smart Grid*, vol. 12, no. 3, pp. 2601–2610, May 2021.

CHANGCHENG LI was born in Fuyu, Jilin Province, China, in 1978. He received the B.S. degree in computer science and technology and the M.S. degree in computer application technology from Beihua University, Jilin, China, in 2003 and 2012, respectively. He is currently pursuing the D.E. degree in computer application technology with the Harbin University of Science and Technology, Heilongjiang, China.

From 2001 to 2003, he was worked at the Computer Center, Beihua University. Since 2004, he has been a Lecturer with the Electrical and Information Engineering College, Jilin Agricultural Science and Technology University. He has authored more than 20 articles. His research interests include signal processing, agriculture Internet of Things, wireless sensor networks, and codes algorithm for hyperspectral signals.

Mr. Li's research project was awarded the Second Prize by Jilin Science and Technology Bureau, in 2018. He was given the Award for Excellence by Jilin Agricultural Science and Technology University, in 2008.

DEYUN CHEN was born in Harbin, Heilongjiang, China. He received the D.E. degree in computer application technology from the Harbin University of Science and Technology, Heilongjiang.

He is currently a Professor, a Doctoral Advisor, and the Dean of the School of Computer Science and Technology, Harbin University of Science and Technology. He has authored more than 200 articles. His research interests include detection and imaging technology, image processing, and pattern recognition algorithm.

CHENGJUN XIE was born in Wangqing County, Jilin Province, China, in 1962. He received the B.S. degree in physics and the M.Ed. degree in physics education from Northeast Normal University, Changchun, and the D.E. degree in optical engineering from the Chinese Academy of Sciences, Beijing.

He is currently the Dean of the College of Computer Science and Technology (Software Institute), Beihua University, Jilin, as well as a Professor and a Doctoral Advisor with Beihua University. He has authored more than 100 articles. His research interests include signal processing and codes algorithm of hyperspectral signal.

Dr. Xie is an Expert Reviewer of National Natural Science Foundation of China, the Director of Association of Fundamental Computing Education in Chinese Universities, the Vice President of Jilin Society of Image and Graphics, the Managing Director of Jilin Computer Federation, the leader of teaching team for computer science courses awarded the Outstanding Teaching Team in Jilin Province, and the Director of Experimental Teaching Center for Computer Science and Technology (approved as Provincial Experimental Teaching Demonstration Center). He wins the title of Young and Middle-Aged Science and Technology Leading Talents with Distinguished Contribution and the Top-Notch Innovator in Jilin Province.

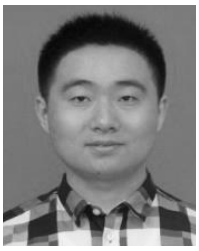

YILONG GAO was born in 1991. He received the Ph.D. degree from the School of Information Science and Engineering, Linyi University. He is currently a Lecturer with the School of Information Science and Engineering, Linyi University. His main research interests include intelligent computing, data processing, and network optimization.

JINRUI LIU received the B.E. degree from the Jilin University of Agricultural Science and Technology, in 2022, where he is currently pursuing the bachelor's degree in electrical and information engineering. Has a national patent invention right. His research interests include network engineering and information security.